SINGLE-SPIRAL-VORTEX MODEL FOR A CAVITATING ELASTIC CURVILINEAR FOIL

A. Y. ZEMLYANOVA[†] AND Y. A. ANTIPOV[‡]
[†] Department of Mathematics, Texas A&M University
College Station TX 77843
[‡]Department of Mathematics, Louisiana State University
Baton Rouge LA 70803

Abstract

A two-dimensional nonlinear inverse fluid-structure interaction problem for a curvilinear elastic hydrofoil is considered. A cavity formed behind the foil is modeled according to the single-spiral-vortex model by Tulin. The fluid-structure problem is decoupled by the method of successive approximations. For the cavitation problem, the foil is modeled as a polygon. The method of conformal mappings and the Riemann-Hilbert problem is employed at this stage. The classical detachment mechanism for a smooth arc is satisfied for the polygon approximately. The deformation of the smooth foil is described by the governing equations of the thin shell theory with the clamped-clamped boundary conditions. The loading acting on the middle surface of the foil is prescribed as the difference between the fluid and vapor pressure computed in the fluid problem. Numerical results include those for the cavity profile, the drag coefficient, the pressure distribution, the speed, and the displacements of the elastic foil.

1 Introduction

Cavitation in fluids is the vaporization of the liquid when pressure drops below the saturation pressure of the liquid. Many engineering machineries deal with appearance and disappearance of cavitation that causes noise, vibrations and erosion. Finite cavity flow has attracted much mathematical interest and provided valuable information for many naval engineering applications including the design and analysis of propellers and hydrofoil systems [11], [8]. Extensive review of the literature may be found in [9], [17], [33], [29], [18], [10], [6], [15].

Mathematical methods used in the cavitation theory include the complex variables technique [18], the boundary integral method [22], the panel method [19] and the Reynolds Average Navier-Stokes (RANS) code. In spite of the fact that many effects due to viscosity are neglected in the free-streamline theory, methods developed for this theory accurately predict drag, lift and the profile of the cavity behind a hydrofoil. The complex variable methods are computationally efficient, which makes them attractive to optimization based design problems arising in the study of cavitating flow. To distinguish any flow in a liquid involving a trailing gas-filled cavity from partial cavitating flow when a cavity is closed on the boundary of a hydrofoil, in 1944 Posdunin (see for example [32]) proposed to call the former flow as supercavitatng flow. Models of supercavitating flow include the Kirchhoff-Joukowsky open wake model, the Riabouchinsky image model, the

Efros-Gilbarg-Rock-Kreisel re-entrant jet model [33], and the two spiral-vortex models by Tulin [32]. The Kirchhoff-Joukowsky open wake model and the Schwarz-Christoffel mapping for the analysis of wake flow past a polygonal obstacle were used in [13]. The Tulin double-spiral-vortex model was applied for the analysis of a cavitating foil beneath a free surface in [24], and in a plane in [7]. This Tulin model was also employed for the design of a numerical scheme for an arbitrary shape cavitating foil in [16]. For simply-connected flow domains, the Tulin nonlinear single-spiral-vortex model was applied in [25], [18] and [2]. Recently, this nonlinear model by Tulin and the method of conformal mappings were generalized for the case of multiply connected free boundary domains in [1], [3], [4], [5]. For these purposes, the method based on the theory of Riemann surfaces and automorphic functions was developed.

If the cavitating hydrofoil is not a polygon, except for the case when the velocity module is prescribed in the foil as a function of the arc length [28], the hodograph method does not give the exact profile of the cavity. For a circular rigid hydrofoil cavitating according to the Kirchhoff-Joukowsky open wake model, a nonlinear integral equation was derived in [23]. The Tulin single-spiral-vortex model problem was analyzed for a cambered rigid foil in [25] and for a circular rigid arc in [18], [30], where a conformal mapping of the interior of a semi-circle into the flow domain was constructed in a series-form, and the coefficients of the series were found by the collocation method and an iterative procedure.

Only a few results on the analysis of cavitating elastic hydrofoils are available in the literature. They include approximate solutions of the Kirchhoff-Joukowsky open wake model problems for an elastic plate and an elastic shell with clamped-free edges in a polygonal tunnel [20], [21]. The boundary integral method developed in [34] for supercavitating and surface-piercing rigid propellers was recently generalized for the elastic case [35].

In this paper we aim to approximately solve the model problem on supercavitating flow past a curvilinear elastic hydrofoil. The Tulin single-spiral-vortex closure mechanism is adopted. The deformation of the hydrofoil is governed by the thin shell theory equations [27]. The method to be proposed is based on the idea of successive approximations. First, the curvilinear hydrofoil is approximated by a rigid polygon. The problem of the cavitation theory is solved by the method of conformal mappings by generalizing the solution for a straight hydrofoil [3] to a polygon. Next, by increasing the number of polygon vertices, an approximate solution for an arc is found, and fluid pressure on the foil is computed. The difference between the external and internal pressure acting on the foil defines the loading on the elastic foil. By deriving the Green's function for the clamped edges of the elastic shell we derive the solution to the elastic problem. This solution defines the deformed profile of the foil, and the cavitation problem is solved for a new polygon that approximates the deformed foil.

2 A thin flexible hydrofoil of an arbitrary shape

2.1 Formulation

An elastic thin curvilinear hydrofoil and a cavity behind are shown in the physical $z = (x_1, x_2)$-plane of Figure 1. The wetted surface of the foil is B_1B_n and a cavity is formed by two curves B_1C_+ and B_nC_-. The flow is two-dimensional, incompressible and irrotational, and the gravity is neglected. As $x_1 = -\infty$, the velocity of the flow is prescribed, $\mathbf{V} = (V_\infty, 0)$. It is assumed that the flow branches at a stagnation point A of the wetted part of the foil. The upper and lower branches of the same streamline smoothly separate from

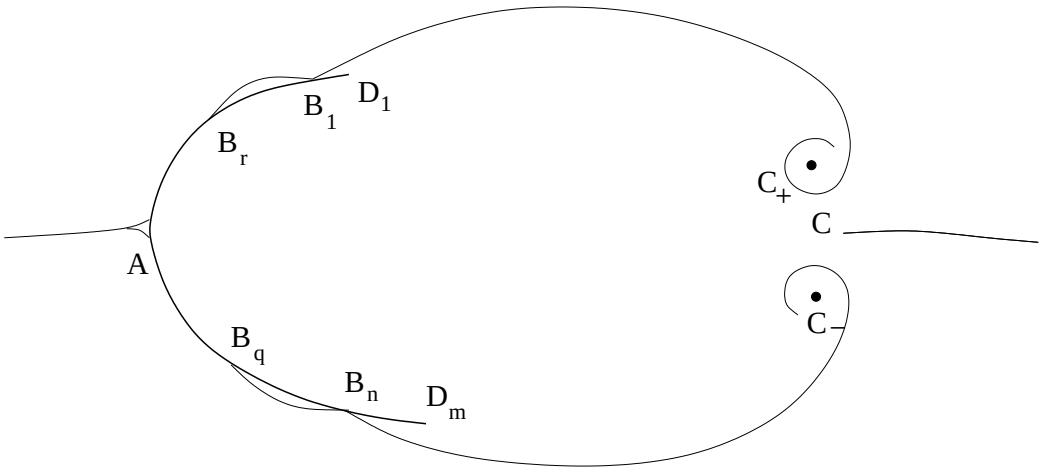

Figure 1: A supercavitating elastic curvilinear hydrofoil.

the foil at some points B_1 and B_n to be determined. The upper and lower streamlines spiral at the points C_+ and C_-. All the five points, A, B_1, B_n, C_+, and C_-, are unknown a priori. The cavity closure mechanism is that described by the Tulin single-spiral-vortex model. Mathematically, it leads to the following asymptotics of logarithm of the conjugate complex velocity $dw/dz = V_1 - iV_2$ [32]

$$\log \frac{dw}{dz} \sim -K((w - w(C))^{-1/2}), \quad z \to C, \quad -\pi \le \arg[w(z) - w(C)] \le \pi. \tag{2.1}$$

Here, $\mathbf{V} = (V_1, V_2)$ is the velocity vector, K is a positive constant, $w(z) = \phi(z) + i\psi(z)$, ϕ is the velocity potential, and ψ is the stream function. The function $w(z)$, the complex velocity potential of the flow, is analytic in the flow domain $\tilde{\mathcal{D}}$. The point C is a point (say, the midpoint) in the segment C_+C_-. The presence of the two partial cavities B_rB_1 and B_qB_n in Figure 1 is confirmed by numerical tests: it turns out that in the segments B_rB_1 and B_qB_n, pressure is lower than the vapor pressure in the cavity, while the speed V in is greater than the speed in the cavity boundary.

The cavity pressure p_c and the speed on the boundary of the cavity, V_c, are constant and prescribed: $V_c = \sqrt{\sigma + 1}V_\infty$, where $\sigma = 2(p_\infty - p_c)(\rho V_\infty^2)^{-1}$ is the cavitation number, ρ is the liquid density, and p_∞ is the pressure as $x_1 = -\infty$. In the boundary of the foil and the cavity, the function $w(z)$ satisfies the following boundary conditions:

$$\begin{gathered} \operatorname{Im} w(z) = K_0, \quad z \in L, \quad K_0 = \text{const}, \\ \left|\frac{dw}{dz}\right| = V_c, \quad z \in B_1C_+ \cup B_nC_-, \quad \arg\frac{dw}{dz} = \beta(z), \quad z \in B_1B_n, \end{gathered} \tag{2.2}$$

where L comprises the wetted boundary of the foil B_1B_n and the boundary of the cavity $B_1C_+ \cup B_nC_-$, and $\beta(z)$ is an unknown function to be determined.

The hydrofoil is assumed to be elastic, and the ratios h/l and h/R are small in comparison with unity. Here h is the thickness of the foil, l is its length, and R is the principal radius of curvature of the middle surface $x_1 = f_1(\alpha)$, $x_2 = f_2(\alpha)$ $(0 \le \alpha \le \alpha_*)$, $-\infty < x_3 < \infty$ of the foil. In what follows we shall be content to prescribe the deformation of the hydrofoil by the equations of thin cylindrical shells [27]

$$\frac{T'}{\mathcal{A}} + \frac{N}{R} = 0, \quad \frac{N'}{\mathcal{A}} - \frac{T}{R} + q_n - p_c = 0, \quad \frac{M'}{\mathcal{A}} - N = 0, \tag{2.3}$$

where $f' = \frac{df}{d\alpha}$, $\mathcal{A} = ds/d\alpha$ is the Lamé parameter, that is the increase of the arc length s along the line $x_1 = f_1(\alpha)$, $x_2 = f_2(\alpha)$, $0 < \alpha < \alpha_*$. The function T is the extensional force, N is the transverse shear force, M is the bending moment, q_n is the water pressure on the foil, and $q_n - p_c$ is the external force per unit length acting on the middle surface of the foil. The force T and the moment M are expressed through the strain ε and the change κ of curvature of the middle surface by $T = \lambda_0\varepsilon, \quad M = \lambda_1\kappa$. Here,

$$\lambda_0 = \frac{Eh}{1-\nu^2}, \quad \lambda_1 = \frac{Eh^3}{12(1-\nu^2)},$$

$$\varepsilon = \frac{u_\tau'}{\mathcal{A}} + \frac{u_n}{R}, \quad \kappa = \frac{\varphi'}{\mathcal{A}}, \quad \varphi = -\frac{u_n'}{\mathcal{A}} + \frac{u_\tau}{R}, \tag{2.4}$$

E is Young's modulus, ν is the Poisson ratio, u_τ and u_n are the tangential and normal displacements, respectively, and φ is the angle of rotation. It will be convenient to rewrite the governing equations in terms of the two displacements

$$\left(\frac{u_\tau'}{\mathcal{A}} + \frac{u_n}{R}\right)' - \frac{\lambda_1}{\lambda_0 R}\left[\frac{1}{\mathcal{A}}\left(\frac{u_n'}{\mathcal{A}} - \frac{u_\tau}{R}\right)'\right]' = 0,$$

$$\left\{\frac{1}{\mathcal{A}}\left[\frac{1}{\mathcal{A}}\left(\frac{u_n'}{\mathcal{A}} - \frac{u_\tau}{R}\right)'\right]'\right\}' + \frac{\lambda_0\mathcal{A}}{\lambda_1 R}\left(\frac{u_\tau'}{\mathcal{A}} + \frac{u_n}{R}\right) = \frac{\mathcal{A}(q_n - p_c)}{\lambda_1}, \quad 0 < \alpha < \alpha_* \tag{2.5}$$

If the edges $\alpha = 0$ and $\alpha = \alpha_*$ are clamped, then both displacements u_τ and u_n and the angle of rotation φ vanish at the edges. This implies the following boundary conditions

$$u_\tau = u_n = u_n' = 0, \quad \alpha = 0, \alpha_*. \tag{2.6}$$

The problem is nonlinear for several reasons. First, it is a free boundary problem since the boundary of the cavity is unknown. Second, the angle $\beta(z)$ is unknown, and the boundary of the foil is defined by the solution of the elastic problem (2.5), (2.6). On the other hand, the pressure q_n is unknown either and should be recovered from the solution of the fluid mechanics problem (2.1), (2.2). Finally, the singular points A, B_1, C_+, C_-, and B_n are unknown. They should be determined through the solution of the coupled fluid-solid interaction problem.

3 A rigid polygonal supercavitating hydrofoil: a cavitation problem

In this section we shall construct an exact solution to the Tulin single-spiral-vortex model for a polygonal rigid hydrofoil. If the number of vertices is large enough, then the solution approximates the exact solution of the problem for a rigid arc. This solution will be used in the next section as the initial approximation in the method of successive approximations for an elastic circular hydrofoil.

Consider a cavitating hydrofoil in the shape of a convex (with respect to the cavity) m-polygon $D_1D_2\dots D_m$. Assume that the wetted part of the foil is $B_1B_2\dots B_n$, where $B_j = D_{m'+j}$, $j = 1, 2, \dots, n$, $1 \le m' + 1 < m' + n \le m$. The points B_1 and B_n are to be determined from the conditions which guarantee the smooth separation of the jets from the hydrofoil. This model admits integrable singularities of the velocity at the vertices B_j ($j = 2, \dots, n-1$) of the wetted part of the polygonal foil.

Let the stagnation point A lie in the segment B_kB_{k+1}, where k $(1 \le k \le n-1)$ is to be determined. Then $\beta(z) = \arg dw/dz$ in (2.2) is a piece-wise constant function given by

$$\beta(z) = \begin{cases} -\beta_j & z \in B_jB_{j+1},\ j = 1, \dots, k-1, \\ \pi - \beta_j, & z \in B_jB_{j+1},\ j = k+1, \dots, n-1, \end{cases} \tag{3.1}$$

and

$$\beta(z) = \begin{cases} -\beta_k, & z \in B_kA, \\ \pi - \beta_k & z \in AB_{k+1}, \end{cases} \tag{3.2}$$

where $0 < \beta_j < \pi$ and

$$\beta_j = \begin{cases} \tan^{-1}(y_{j+1} - y_j)/(x_{j+1} - x_j), & x_{j+1} < x_j, \\ \pi + \tan^{-1}(y_{j+1} - y_j)/(x_{j+1} - x_j), & x_{j+1} > x_j, \\ \pi/2, & x_{j+1} = x_j, \end{cases} \qquad j = 1, 2, \dots, n-1. \tag{3.3}$$

We do not consider the case $-\pi < \beta_j < 0$ because it is physically infeasible.

To solve the problem, we employ the method of conformal mappings. Let $z = f(\zeta)$ be a conformal mapping of the exterior of the unit circle, $|\zeta| > 1$, onto the flow domain such that the circle $\mathcal{C} = \{\zeta : |\zeta| = 1\}$ is mapped onto the contour $\mathcal{L} = W \cup B_1CB_n$ which comprises the wetted part of the polygonal hydrofoil, $W = B_nB_{n-1} \dots B_1$ and the boundary of the cavity $B_1C_+CC_-B_n$. The positive direction is chosen such that the flow domain is on the left. We shall reconstruct this mapping assuming that the infinite point of the parametric ζ-plane is mapped into the infinite point $z = \infty$ of the physical plane. Assume also that the points B_j, A, and C are the images of some points b_j, a, and c in the unit circle $\mathcal{C}$. The points in the circle $\mathcal{C}$ follow each other in the same order as their images are located in the contour $\mathcal{L}$. The preimages of the points C_+ and C_- are the left and the right limit points of the point c. As in most two-dimensional free boundary problems, we seek the conformal mapping in the form

$$\frac{df}{d\zeta} = V_\infty^{-1}\omega_0(\zeta)e^{-\omega_1(\zeta)}, \tag{3.4}$$

where $\omega_0(\zeta) = dw/d\zeta$, $V_\infty e^{\omega_1(\zeta)} = dw/dz$. The function $\omega_0(\zeta)$ is independent of the points b_j. It is analytic in the domain $|\zeta| > 1$ and has to have simple zeros at the points a and c. On the unit circle, it satisfies the boundary condition

$$\omega_0(\zeta) = -\frac{1}{\zeta^2}\overline{\omega_0(\zeta)}, \quad \zeta = \xi \in \mathcal{C}. \tag{3.5}$$

The solution of this problem is the following rational function [3]:

$$\omega_0(\zeta) = \frac{iN(\zeta - a)(\zeta - c)}{\sqrt{ac}\zeta^2}. \tag{3.6}$$

Here, N is an arbitrary real constant, and $\sqrt{ac}$ is the value of a fixed branch of the square root.

Now we determine the second function $\omega_1(\zeta)$. This function is also analytic in the exterior of the unit circle $\mathcal{C}$. On the circle itself, it satisfies the Hilbert boundary conditions

$$\begin{aligned} \operatorname{Re}\omega_1(\zeta) &= \frac{1}{2}\ln(\sigma + 1), \quad \zeta \in b_1cb_n, \\ \operatorname{Im}\omega_1(\zeta) &= g_0(\zeta), \quad \zeta \in b_nb_{n-1} \dots b_1, \end{aligned} \tag{3.7}$$

where

$$g_0(\zeta) = \begin{cases} -\beta_j, & \zeta \in b_j b_{j+1},\ j = 1, \dots, k-1, \\ -\beta_k, & \zeta \in b_k a, \\ \pi - \beta_k, & \zeta \in a b_{k+1}, \\ \pi - \beta_j, & \zeta \in b_j b_{j+1},\ j = k+1, \dots, n-1. \end{cases} \tag{3.8}$$

By using the Schwarz symmetry principle, we extend the definition of the function $\omega_1(\zeta)$ to the whole ζ-plane:

$$\omega_1(\zeta) = \overline{\omega_1(1/\bar{\zeta})}, \quad \zeta \in \operatorname{int} \mathcal{C}. \tag{3.9}$$

This enables us to rewrite the Hilbert problem (3.7) as the Riemann-Hilbert problem

$$\omega_1^+(\xi) = \mathcal{G}(\xi)\omega_1^-(\xi) + g(\xi), \quad \xi \in \mathcal{C}, \tag{3.10}$$

subject to the symmetry condition (3.9). Here, $\omega_1^+(\xi)$ is the limiting value of the function $\omega_1(\zeta)$ as $\zeta \to \xi \in \mathcal{C}$ and $|\zeta| > 1$, and $\omega_1^-(\xi) = \overline{\omega_1^+(\xi)}$,

$$\mathcal{G}(\xi) = \begin{cases} -1, & \xi \in b_1 c b_n, \\ 1, & \xi \in b_n a b_1, \end{cases} \qquad g(\xi) = \begin{cases} \ln(\sigma + 1), & \xi \in b_1 c b_n, \\ 2i g_0(\xi), & \xi \in b_n a b_1, \end{cases} \tag{3.11}$$

Due to the Tulin model (2.1), the function $\omega_1(\zeta)$ has a simple pole at the point $z = c$. At the points b_2, $b_3, \dots, b_{n-1}$, this function has logarithmic singularities. At the infinite point of the ζ-plane, it vanishes.

A closed-form solution to the symmetric Riemann-Hilbert problem (3.9) to (3.11) can be constructed by following the technique [3]. It has the form

$$\omega_1(\zeta) = \chi(\zeta) \left[\frac{\ln(\sigma + 1)}{4\pi i} \int\limits_{b_1 c b_n} \frac{\xi + \zeta}{\xi - \zeta} \frac{d\xi}{\xi \chi^+(\xi)} + \frac{1}{2\pi} \int\limits_{b_n a b_1} \frac{\xi + \zeta}{\xi - \zeta} \frac{g_0(\xi) d\xi}{\xi \chi(\xi)} \right], \tag{3.12}$$

where $\chi(\zeta)$ is a solution to the factorization problem $\mathcal{G}(\xi) = \chi^+(\xi)/\chi^-(\xi)$, $\xi \in \mathcal{C}$,

$$\chi(\zeta) = \left(\frac{c^2}{b_1 b_n} \right)^{1/4} \frac{[(\zeta - b_1)(\zeta - b_n)]^{1/2}}{\zeta - c}. \tag{3.13}$$

Here, $\chi(\zeta)$ is the branch of the square root chosen by the condition $[(\zeta - b_1)(\zeta - b_n)]^{1/2} \sim \zeta$, $\zeta \to \infty$. It is a single-valued analytic function in the ζ-plane cut along the arc $b_n c b_1$ of the circle $\mathcal{C}$. Analysis of the function $\omega_1(\zeta)$ shows that it vanishes at the points $\zeta = b_1$ and b_n, has logarithmic singularities at the point $b_2, \dots, b_{n-1}$ and a simple pole at the point $\zeta = c$.

It will be convenient to represent the function $df/d\zeta$ in the form

$$\frac{df}{d\zeta} = \frac{N}{V_\infty} \mathcal{F}(\zeta), \tag{3.14}$$

where

$$\mathcal{F}(\zeta) = \frac{i(\zeta - a)(\zeta - c)}{\sqrt{ac}\,\zeta^2} e^{-\omega_1(\zeta)}. \tag{3.15}$$

The expression (3.14) possesses $n + 3$ unknown parameters. They are the real coefficient N and $n + 2$ points a, c, $b_1, b_2, \dots, b_n$ in the unit circle $\mathcal{C}$. In the simply connected case a conformal mapping is defined up to three arbitrary real parameters. We have fixed two parameters (the infinite point of the parametric plane is mapped into the infinite point of

the physical plane). Therefore, one of the points in the circle $\mathcal{C}$ can be chosen arbitrarily. Let $a = -1$. Determine next the conditions for the determination of the other parameters. The function $\omega_1(\zeta)$ must vanish at the infinite point. This is guaranteed if

$$\frac{\ln(\sigma+1)}{2i}\int\limits_{b_1cb_n}\frac{d\xi}{\xi\chi^+(\xi)}+\int\limits_{b_nab_1}\frac{g_0(\xi)d\xi}{\xi\chi(\xi)}=0. \tag{3.16}$$

Since the function $\chi(\zeta)$ is pure imaginary on the arc b_ncb_1 and real on the arc b_1ab_n, the condition (3.16) is a real equation. On account of continuity of the flow domain,

$$\int_{\mathcal{C}'}\mathcal{F}(\zeta)d\zeta=0, \tag{3.17}$$

where $\mathcal{C}'$ is an arbitrary simple closed contour such that the unit circle $\mathcal{C}$ lies in its interior. Choose $\mathcal{C}'$ as a circle $|\zeta| = r'$, $r' > 1$. The complex equation (3.17) brings two extra real equations. The remaining $n-1$ equations are the following geometric conditions:

$$\frac{N}{V_\infty}\,\mathrm{Im}\int\limits_{b_jb_{j+1}}\mathcal{F}(\xi)d\xi=\lambda\sin\beta_j,\quad j=1,2,\dots,n-1. \tag{3.18}$$

The solution will not be completed if we do not determine the detachment points B_1 and B_n. Because the wetted side of the foil is a part of a polygon, the flow separates at two vertices of the hydrofoil $D_1D_2\dots D_m$. To define these two vertices, we apply the Brillouin-Villat separation condition [9], [10]. For a smooth hydrofoil, at the detachment points the curvatures of the hydrofoil and the cavity are the same. Equivalently, based on formula (3.4) and the analysis of the Cauchy integral (3.12) we conclude that for a smooth hydrofoil the detachment points B_1 and B_n can be determined from the conditions

$$\omega_1'(\zeta)=O(1),\quad z\to B_1\quad\text{and}\quad z\to B_n. \tag{3.19}$$

Here, z approaches the detachment points along the cavity boundary. In the case of a polygonal hydrofoil, in general, these conditions cannot be achieved. Instead,

$$\omega_1'(\zeta)\sim-\frac{iN_j^\pm}{2}(z-D_j^\pm)^{-1/2},\quad z\to D_j^\pm,\quad j=1,2,\dots,m, \tag{3.20}$$

where $N_j^\pm$ are some real, in general non-zero, constants, and D_j^+ and D_j^- are possible upper and lower detachment points. Therefore, the detachment points $B_1 = D_s^+$ and $B_n = D_t^-$ can be determined by finding the minimum element M_{st} among all possible numbers $M_{kj}=\sqrt{(N_k^+)^2+(N_j^-)^2}$, $k, j = 1, 2, \dots, m$.

As a numerical experiment, we consider a regular polygonal hydrofoil inscribed in a circular arc passing through the origin $(0, 0)$ with the ending points $D_1 = (1, 1)$ and $D_m = (1, -1)$. We choose the number of vertices to be even, $m = 2l$. The zero-angle-of-attack assumption enforces the stagnation point A to be the midpoint of the segment D_lD_{l+1} and $N_1 = N_{2l}$. Figure 2 shows the results of computations for three different choices of the pairs of detachment points in the case when $m = 12$, $V_\infty = 1$, and $\sigma = 0.5$. From the symmetry of the hydrofoil it follows that $N_j^+ = N_j^- = N_j$. The solid line corresponds to the pair (D_2, D_{11}) which meets the criterion for the choice of the detachment points (the coefficient N_2 is the smallest among all the numbers N_j $(j = 1, 2, \dots, 6)$). The other two lines, lines 1 and 3, corresponds to the pairs (D_1, D_{12}) and (D_3, D_{10}). It is seen that the finding of the detachment points is crucial for the definition of the cavity profile.

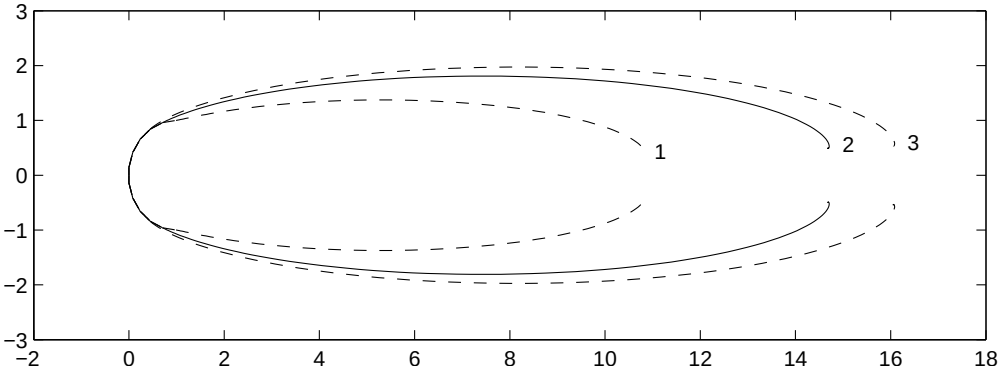

Figure 2: The cavity profile (the solid line) for a rigid polygonal hydrofoil and mock boundaries (lines 1 and 3) when $m = 12$, $V_\infty = 1$, and $\sigma = 0.5$.

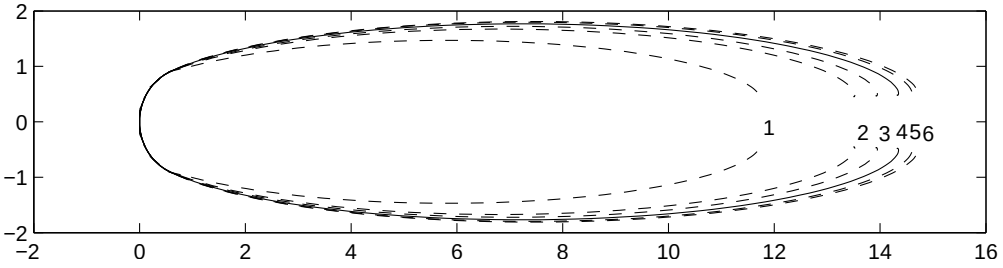

Figure 3: The cavity profile for different approximations of a rigid circular arc by polygonal hydrofoils ($V_\infty = 1$, $\sigma = 0.5$).

m	Separation points	C_X	$\pm\beta_c$	Cavity length
8	D_1, D_8	0.600881	$\pm 0.5\pi$	11.711497
12	D_2, D_{11}	0.740330	$\pm 0.590509\pi$	14.682922
16	D_2, D_{15}	0.684192	$\pm 0.566667\pi$	13.499925
20	D_3, D_{18}	0.735119	$\pm 0.60526\pi$	14.574629
24	D_3, D_{22}	0.704260	$\pm 0.586956\pi$	13.924080
30	D_4, D_{27}	0. 723234	$\pm 0.603448\pi$	14.323796

Table 1: The drag coefficient C_X, the angles of detachment $\pm\beta_c$, and the cavity length for some numbers of the hydrofoil vertices ($V_\infty = 1$, $\sigma = 0.5$).

The possibility of reconstruction of the cavity profile for a circular arc has also been investigated. Figure 3 shows the cavity shape for the polygonal hydrofoils with different number of the vertices. This was accomplished by computing the cavity profile for $m = 8, 12, 16, 20, 24,$ and 30 (the lines 1, 6, 2, 5, 3 and 4, respectively). By increasing further the number of points it is possible to achieve the convergence, and the actual profile of the cavity behind the circular arc is expected to be between the lines 3 and 4. The detachment points, the drag coefficient

$$C_X = \mathrm{Re}\left\{\frac{i}{2R}\int\limits_{\mathcal{L}}(1+\sigma-e^{2Re\omega_1(\zeta)})e^{-\omega_1(\zeta)}\omega_0(\zeta)d\zeta\right\}, \tag{3.21}$$

the cavity length, the polar coordinates of the detachment points, and the cavity length for some numbers of the vertices are shown in Table 1. In (3.21), the contour $\mathcal{L} = b_n b_1$ is the preimage of the wetted part of the hydrofoil.

The nonlinear system of equations (3.16) to (3.18) has been solved numerically by the Newton method. To remove the natural constrains for the unknowns we introduce the variables [31]

$$t_1 = \ln\frac{\theta_2-\theta_1}{\theta_1-\theta_c}, \quad t_n = \ln\frac{\theta_c-\theta_n}{\theta_n-\theta_{n-1}},$$

$$t_j = \ln\frac{\theta_{j+1}-\theta_j}{\theta_j-\theta_{j-1}}, \quad 2\le j\le k-1, \quad k+2\le j\le n-1,$$

$$t_k = \ln\frac{\pi-\theta_k}{\theta_k-\theta_{k-1}}, \quad t_{k+1} = \ln\frac{\theta_{k+2}-\theta_{k+1}}{\theta_{k+1}+\pi},$$

$$t_c = \ln\frac{\theta_1-\theta_c}{\theta_c-\theta_n}, \tag{3.22}$$

where $b_j = e^{i\theta_j}$, $j = 1, 2, \ldots, n$, $c = e^{i\theta_c}$ and the polar angles θ_j and θ_c are chosen so that

$$-\pi < \theta_{k+1} < \ldots < \theta_{n-1} < \theta_n < \theta_c < \theta_1 < \ldots < \theta_{k-1} < \theta_k < \pi. \tag{3.23}$$

Having solved the system (3.16) to (3.18) we can find the polar angles as

$$\theta_c = \pi\Delta_0(1 + e^{t_{k+1}} + e^{t_{k+1}+t_{k+2}} + \ldots + e^{t_{k+1}+\ldots+t_n} - e^{t_c+t_{k+1}+\ldots+t_n}$$

$$-e^{t_1+t_c+t_{k+1}+\ldots+t_n} - \ldots - e^{t_1+\ldots+t_k+t_c+t_{k+1}+\ldots+t_n}),$$

$$\theta_j = \pi\Delta_0(1 + e^{t_{k+1}} + e^{t_{k+1}+t_{k+2}} + \ldots + e^{t_{k+1}+\ldots+t_n} + e^{t_c+t_{k+1}+\ldots+t_n}$$

$$+e^{t_1+t_c+t_{k+1}+\ldots+t_n}+\ldots+e^{t_1+\ldots+t_{j-1}+t_c+t_{k+1}+\ldots+t_n}-e^{t_1+\ldots+t_j+t_c+t_{k+1}+\ldots+t_n}$$
$$-\ldots-e^{t_1+\ldots+t_k+t_c+t_{k+1}+\ldots+t_n}),\quad 1\le j\le k,$$
$$\theta_{j+k}=\pi\Delta_0(1+e^{t_{k+1}}+\ldots+e^{t_{k+1}+\ldots+t_{k+j-1}}-e^{t_{k+1}+\ldots+t_{k+j}}-\ldots-e^{t_{k+1}+\ldots+t_n}$$
$$-e^{t_c+t_{k+1}+\ldots+t_n}-\ldots-e^{t_1+\ldots+t_k+t_c+t_{k+1}+\ldots+t_n}),\ \ 1\le j\le n-k, \tag{3.24}$$

where

$$\Delta_0=(1+e^{t_{k+1}}+\ldots+e^{t_{k+1}+\ldots+t_n}+e^{t_c+t_{k+1}+\ldots+t_n}+\ldots+e^{t_1+\ldots+t_k+t_c+t_{k+1}+\ldots+t_n})^{-1}. \tag{3.25}$$

To complete the description of the numerical procedure, we need to write down the the singularity coefficient used in the criterion for the definition of the detachment points. This coefficient is obtained by separating singular and regular parts of the integrals in the formula (3.12). In the symmetric case, the coefficient associated with the vertex B_1 has the form

$$N_1=\left|\frac{df}{d\zeta}\right|^{-1/2}\left\{-\frac{\ln(\kappa+1)}{4\pi i}\left[\int_{\theta_n}^{\theta_1}\left(\sqrt[4]{\frac{c^2}{b_1b_n}}\frac{\sqrt{b_1-b_n}}{b_1-c}\frac{e^{i\varphi}+e^{i\psi}}{e^{i\varphi}-e^{i\psi}}\frac{id\varphi}{\chi_\omega^+(e^{i\varphi})}\right.\right.\right.$$
$$\left.\left.\left.-\frac{2}{\sqrt{-ie^{i\theta_1}}}\frac{d\varphi}{(\varphi-\psi)\sqrt{\theta_1-\varphi}}\right)-\frac{4}{\sqrt{-ie^{i\theta_1}}}\frac{1}{\sqrt{\theta_1-\theta_n}}\right]\right.$$
$$+\frac{\beta_1}{2\pi}\int_{\theta_1}^{\theta_2}\left(\sqrt[4]{\frac{c^2}{b_1b_n}}\frac{\sqrt{b_1-b_n}}{b_1-c}\frac{e^{i\varphi}+e^{i\psi}}{e^{i\varphi}-e^{i\psi}}\frac{id\varphi}{\chi_\omega^+(e^{i\varphi})}-\frac{2}{\sqrt{ie^{i\theta_1}}}\frac{d\varphi}{(\varphi-\psi)\sqrt{\varphi-\theta_1}}\right)$$
$$\left.-\frac{2\beta_1}{\pi\sqrt{ie^{i\theta_1}}}\frac{1}{\sqrt{\theta_2-\theta_1}}+\sqrt[4]{\frac{c^2}{b_1b_n}}\frac{\sqrt{b_1-b_n}}{b_1-c}\int_{b_nb_{n-1}\ldots b_2}g_0(\xi)\frac{\xi+\zeta}{\xi-\zeta}\frac{d\xi}{\xi\chi_\omega^+(\xi)}\right\}, \tag{3.26}$$

where all the branches of the square roots are chosen in the same way as in the function $\chi_\omega(\zeta)$, and the last integral is taken along the arc of the unit circle $b_nb_{n-1}\ldots b_2$.

Figure 4 shows the results of calculations of the drag coefficient C_X for different positions of the detachment angle β_c. The curves practically coincide with those presented in [18], p. 209. The location of the detachment points found is indicated in Figure 4 by the arrows.

The drag coefficient C_X increases with the cavitation number σ. For a rigid hydrofoil, our results (Figure 5) for a polygonal foil with $m=12$ coincide with the ones for a circular foil obtained in the framework of the Kirchhoff-Joukowsky open wake model by Roshko when $\sigma\in(0.1,0.5)$ and by Efros when $\sigma\in(0.1,0.75)$ [14].

4 A thin circular elastic foil with clamped ends: an elastic problem

Let the foil be a thin infinite cylindrical shell whose middle surface is $x_1=r\cos(\alpha+\alpha^\circ)$, $x_2=r\sin(\alpha+\alpha^\circ)$, $-\infty<x_3<+\infty$, where $r=R$, $0<\alpha<\alpha_*$. In this case the Lamé coefficient $\mathcal{A}=R$, and the governing equations (2.5) become

$$(1+\lambda_*)u''+w'-\lambda_*w'''=0,$$
$$\lambda_*(w''''-u''')+u'+w=\frac{R^2}{\lambda_0}(q_n-p_c), \tag{4.1}$$

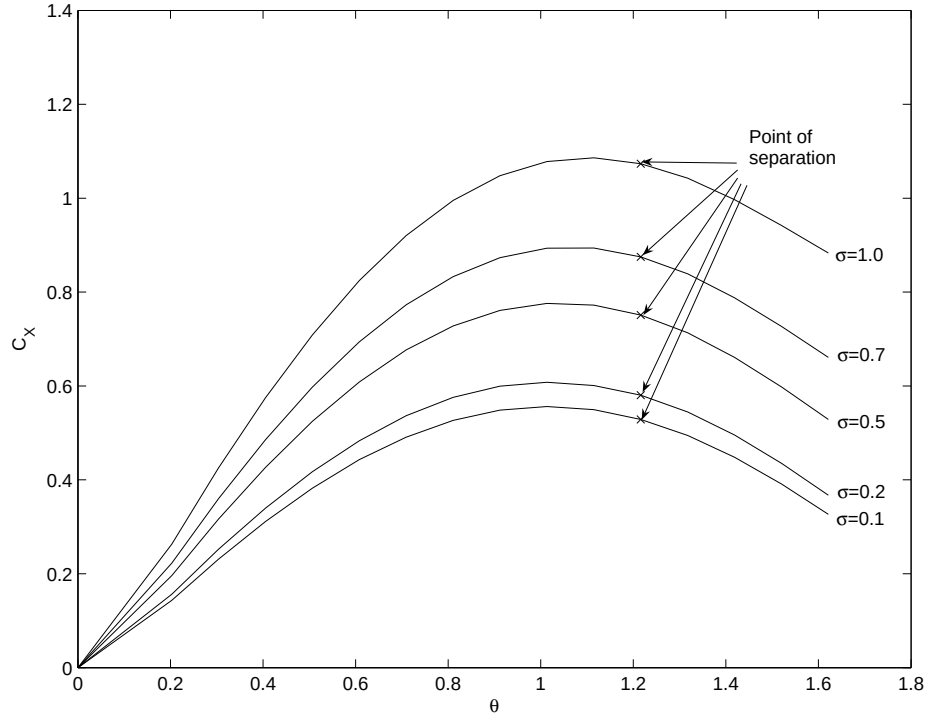

Figure 4: The drag coefficient C_X vs the polar angle θ of the detachment point for different values of the cavitation number σ when $m = 16$ and $V_\infty = 1$.

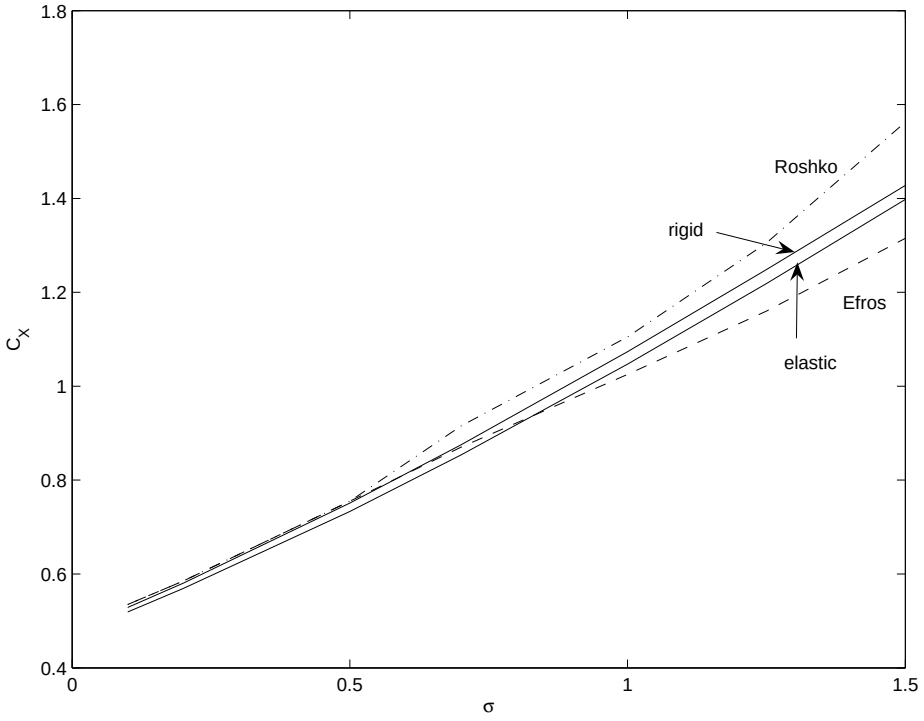

Figure 5: The drag coefficient C_X vs the cavitation number σ.

where $u = u_\tau$ and $w = u_n$ are the tangential and the normal components of the displacement vector, and $\lambda_* = \frac{1}{12}(h/R)^2$. These equations reduce to the fourth order differential equation for the displacement w

$$w'''' + 2w'' + w = \left(1 + \frac{1}{\lambda_*}\right)\left(-C_0 + \frac{q_n - p_c}{\lambda_0}R^2\right). \tag{4.2}$$

and the following equation for the displacement u:

$$u' = \frac{\lambda_* w'' - w}{1 + \lambda_*} + C_0. \tag{4.3}$$

Here, C_0 is an arbitrary constant.

Assume that the edges of the foil are clamped to rigid plates $\alpha = 0$ and $\alpha = \alpha_*$, $-\infty < x_3 < \infty$, fixed in the flow domain. Then the boundary conditions are

$$w(0) = w(\alpha_*) = 0, \quad w'(0) = w'(\alpha_*) = 0, \tag{4.4}$$

and

$$u(0) = u(\alpha_*) = 0. \tag{4.5}$$

The function w can be determined by constructing the Green's function, $G(\alpha, \beta)$, of the boundary value problem (4.2) and (4.4). On using the method [26] we find for $0 \le \alpha \le \beta$

$$\begin{aligned} G(\alpha,\beta) = \frac{1}{\Delta}\{&\cos\beta[-\alpha(1 + 2\beta\alpha_* - 2\alpha_*^2)\cos\alpha + (1 - \beta\alpha + 2\beta\alpha_* - 2\alpha_*^2)\sin\alpha] \\ &+ \sin\alpha[(-1 + \beta\alpha)\cos(\beta - 2\alpha_*) + (\beta - 2\beta\alpha\alpha_* + 2\alpha_*(-1 + \alpha\alpha_*))\sin\beta \\ &-\beta\sin(\beta - 2\alpha_*)] + \alpha\cos\alpha[\cos(\beta - 2\alpha_*) - (\beta - 2\alpha_*)\sin\beta + \beta\sin(\beta - 2\alpha_*)]\}. \end{aligned} \tag{4.6}$$

If $\beta \le \alpha \le \alpha_*$, then the Green's function is given by

$$\begin{aligned} G(\alpha,\beta) = \frac{1}{\Delta}\{&\cos\alpha[\alpha\cos(\beta - 2\alpha_*) + (1 - \beta\alpha + 2\alpha\alpha_* - 2\alpha_*^2 - \cos 2\alpha_*)\sin\beta \\ &+\beta\alpha\sin(\beta - 2\alpha_*)] + \cos\beta[-\cos\alpha(\beta + 2\beta\alpha\alpha_* - 2\beta\alpha_*^2) - (\alpha - \beta)\cos\alpha\cos 2\alpha_* \\ &+\beta\sin\alpha(-\alpha + 2\alpha_* + \sin 2\alpha_*)] + \sin\alpha[\beta\alpha\cos(\beta - 2\alpha_*) \\ &+\sin\beta(\alpha - 2\alpha_* - 2\beta\alpha\alpha_* + 2\beta\alpha_*^2 - \alpha\cos 2\alpha_* - \sin 2\alpha_*)]\}. \end{aligned} \tag{4.7}$$

Here,

$$\Delta = 4(\alpha_*^2 - \sin\alpha_*^2) \tag{4.8}$$

Employing this function furnishes the resulting formula for the displacement w

$$w(\alpha) = -C_1 g(\alpha) + \lambda_2 \int_0^{\alpha_*} G(\alpha,\beta)[q_n(\beta) - p_c]d\beta, \tag{4.9}$$

where

$$C_1 = \left(1 + \frac{1}{\lambda_*}\right)C_0, \quad \lambda_2 = \frac{R^2}{\lambda_0}\left(1 + \frac{1}{\lambda_*}\right),$$

$$g(\alpha) = \int_0^{\lambda_*} G(\alpha,\beta)d\beta. \tag{4.10}$$

Once the normal displacement w is found, the tangential displacement u is defined from equation (4.3) by integration. On satisfying the boundary conditions (4.5) we define

$$u(\alpha) = \frac{1}{1+\alpha_*}\left\{\lambda_* w' + C_1 g^\circ(\alpha) - \lambda_2 \int\limits_0^{\alpha_*} G^\circ(\alpha,\beta)[q_n(\beta) - p_c]d\beta\right\}, \tag{4.11}$$

where

$$g^\circ(\alpha) = \int\limits_0^{\alpha_*} G^\circ(\alpha,\beta)d\beta, \quad G^\circ(\alpha,\beta) = \int\limits_0^{\alpha} G(\alpha_1,\beta)d\alpha_1,$$

$$C_1 = \frac{\lambda_2}{g^\circ(\alpha_*)} \int\limits_0^{\alpha_*} G^\circ(\alpha_*,\beta)[q_n(\beta) - p_c]d\beta. \tag{4.12}$$

5 An elastic circular supercavitating hydrofoil: a fluid-structure interaction problem

On using the two exact solutions presented in the previous sections for a regular rigid cavitating polygon and a circular elastic shell we can develop an approximate procedure for an elastic circular supercavitating hydrofoil. It is assumed that both edges of the foil are clamped. First, we approximately replace the arc by a regular polygon $D_1D_2\dots D_m$, where m is the number of vertices chosen. By the method described in Section 3, we reconstruct the conformal mapping from the exterior of the unit circle $\mathcal{C}$ into the exterior of the domain whose boundary comprises the hydrofoil surface and the cavity boundary. After that we determine the detachment points B_1 and B_n and, therefore, the wetted part, $B_1B_2\dots B_n$ of the foil.

This makes possible to compute the speed V everywhere in the liquid

$$V^2 = \frac{dw}{dz}\overline{\frac{dw}{dz}} = V_\infty^2\left(e^{2\,\mathrm{Re}\,\omega_1(\zeta)}\right). \tag{5.1}$$

On employing the Bernoulli formula

$$q(s) + \frac{\rho}{2}V^2 = p_\infty + \frac{\rho}{2}V_\infty^2, \tag{5.2}$$

we determine fluid pressure

$$q(s) = p_\infty - \frac{\rho V_\infty^2}{2}\left(e^{2\,\mathrm{Re}\,\omega_1(\zeta)} - 1\right). \tag{5.3}$$

Here, s is the length of a segment B_jz, $z \in B_jB_{j+1}$, and

$$s = \int\limits_{b_j}^{\zeta}\left|\frac{df}{d\zeta}\right||d\zeta|, \quad \zeta \in b_jb_{j+1}, \dots j = 1,2,\dots,n-1. \tag{5.4}$$

Next, we use the function $q(s)$ as an approximation of the normal loading q_n in equation (4.1). The normal and tangential displacements of any point in the middle surface of the foil are given by the exact formulas (4.8) to (4.11). What we need, however, is the

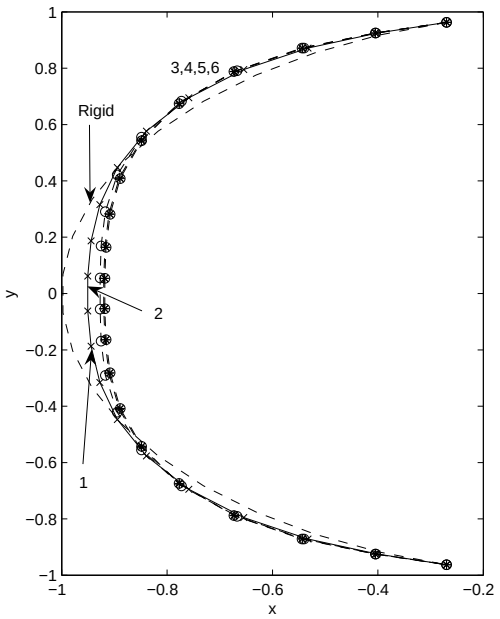

Figure 6: The deformed profile of the cavitating hydrofoil.

displacement vector at the points B_1, $B_2, \ldots, B_n$ only. On knowing this vector, we can correct the positions of the vertices of the polygon.

The third step of the procedure is the solution of the cavitation problem for a new rigid polygon. It will be convenient to introduce new notations, $D'_j = B_j$, $j = 1, 2, \ldots, n$. The wetted part of the foil does not necessarily coincide with that obtained in the first step of the solution. The new detachment points say, B'_1 and $B'_{n'}$, are determined in the same way as the points B_1 and B_n. On the ground of the solution to this new cavitation problem we determine a new approximation of fluid pressure on the external side of the polygon. In the framework of linear theory of thin shells we can assume that the shell is circular and use equations (4.2) and (4.3) again. It is assumed that the iterative process described reaches sufficient accuracy, ε, if

$$\max_{s \in W} |1 - ||\mathbf{u}^{(m)}||/||\mathbf{u}^{(m-1)}||| < \varepsilon, \tag{5.5}$$

where W is the wetted part of the foil, $\mathbf{u} = (u, w)$, $\mathbf{u}^{(m-1)}$ and $\mathbf{u}^{(m)}$ are two successive approximations of the displacement vector $\mathbf{u}$, and $||\mathbf{u}|| = \sqrt{u^2 + w^2}$.

The deformed profile of the elastic semi-arc is shown in Figure 6. It is seen that the largest deformation occurs at the center of the foil. For the test, we chose the Young's modulus as $E = 6 \times 10^7$, Poisson ratio ν as 0.33, the thickness h of the foil as 0.002, and the other parameters as $\sigma = 0.5$, $V_\infty = 1$, and $\rho = 1$. To approximate a half of the circular foil, 12 points were employed, and the cavity started at the tenth point. It is seen that the differences between the profiles obtained in steps 4, 5 and 6 of the approximate method described become invisible.

The dimensionless normal and tangential displacements w/r and u/r for the same data as in Figure 6 are presented in Figure 7. Here,

$$r = \frac{R^2 \rho V_\infty^2}{2\lambda_0} 10^5, \quad R = 1, \tag{5.6}$$

and curves j ($j = 1, 2, \ldots, 6$) correspond to the jth step of the method. The tangential

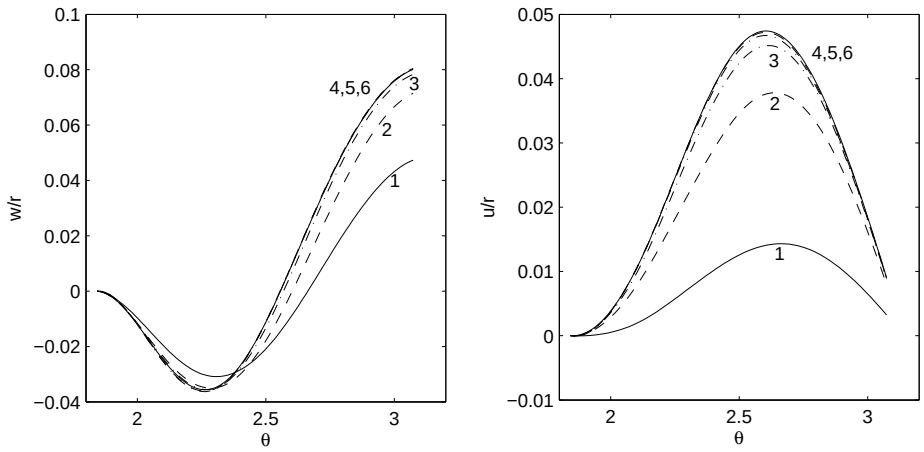

Figure 7: The dimensionless normal (w/r) and tangential (u/r) displacements of the hydrofoil.

displacement u is always nonnegative and vanishes at the center of the arc ($\theta = \pi$) and its ending points. The normal displacement w attains its maximum at the point $\theta = \pi$ (at the center of the foil), decreases in the interval (θ_*, π), attains its minimum, $w_* < 0$, and vanishes at the clamped ends.

Very often in the theory of potential flow, instead of the parametric ζ-plane, the plane (V, Θ), where $V = |dw/dz|$ and $\Theta = \arg dw/dz$, is used. In Figure 8, some streamlines around an elastic hydrofoil and their images in the plane (V, Θ) are given. The image of the streamline which defines the boundary of the cavity is the vertical line $V = V_c$ in the plane (V, Θ). Since $\arg dw/dz$ is a piecewise constant function, the image of the polygonal boundary of the hydrofoil is also a discontinuous function (the images of the cavity and the foil boundaries are not shown in Figure 8).

The external force $q_n - p_c$ per unit length acting on the middle surface of a regular polygonal hydrofoil is shown in Figure 9. The following parameters were employed: $E = 6 \times 10^7$, $\nu = 0.33$, $h = 0.002$, $\sigma = 0.5$, $V_\infty = 1$, $\rho = 1$, and $n = 30$. Our computations showed that the detachment points are D_4 and D_{27}. As it was expected, the maximum of the loading function is attained at the stagnation point. The curve is not smooth. This is explained by the polygonal shape of the foil: at each vertex of the hydrofoil pressure of liquid drops. The increase of the number of vertices leads to the decrease of the amplitudes of the spikes. Another interesting observation to be made is that there are two zones at the ends of the wetted hydrofoil where the liquid pressure drops below the vapor pressure in the cavity. A possible explanation of this phenomenon could be the presence of two thin partial cavities formed by the jets before they break away from the hydrofoil and form the supercavity. The solid line in Figure 9 shows an approximation of the difference $q_n - p_c$ for a rigid and an elastic circular arcs. It is seen that the predicted partial cavities are longer for the elastic hydrofoil. Computations made for the speed V along the boundary of the hydrofoil (rigid and elastic) (Figure 10, the data are the same as in Figure 9) also show that there are two partial cavities close to the point where the jets break away and form a supercavity: the speed V in these zones is greater than the speed V_c in cavity boundary.

Finally, we discuss the effect of elasticity on the drag coefficient, length and width of the supercavity. It turns out that drag coefficient C_X is less for an elastic foil than for the rigid one (Figure 5, the data are the same as in Figure 9). Figures 11 and 12 show

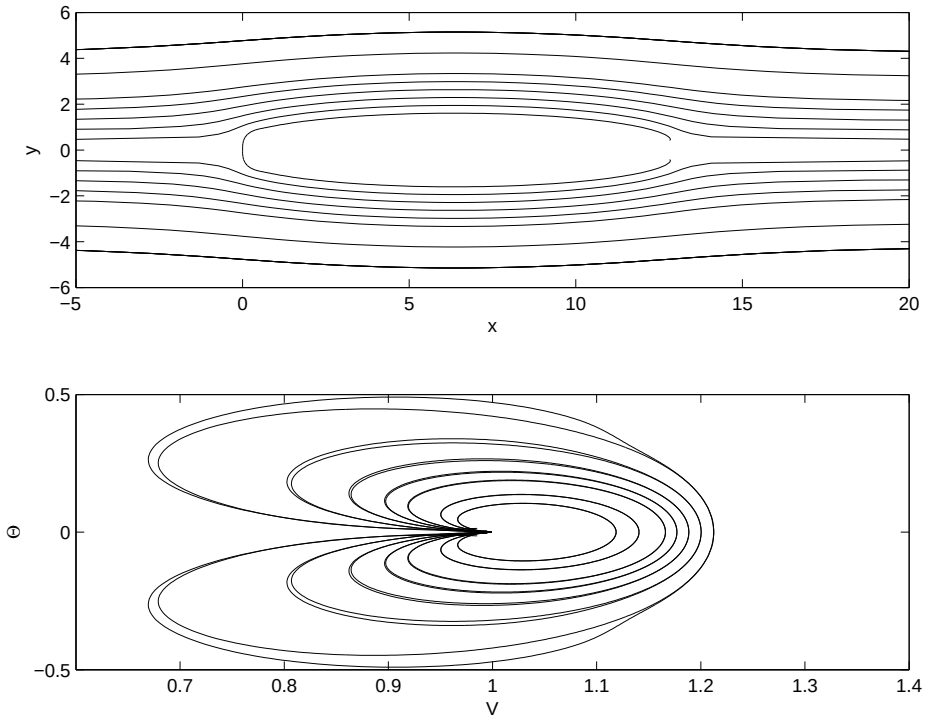

Figure 8: Streamlines around the hydrofoil in the physical plane and in the plane (V, Θ) ($V = |dw/dz|$, $\Theta = \arg dw/dz$).

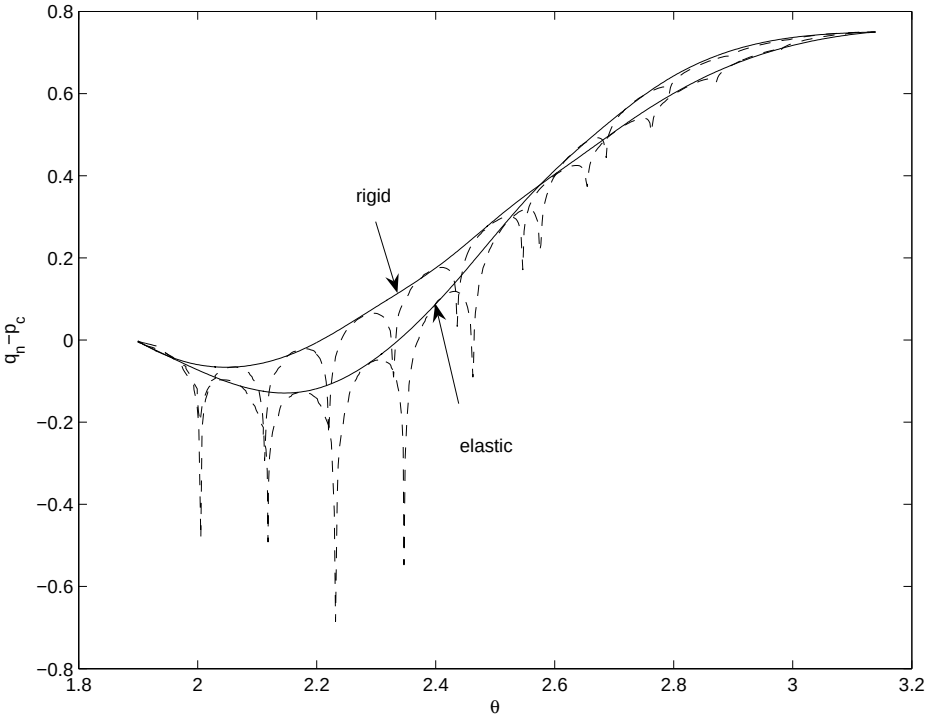

Figure 9: The external force $q_n - p_c$ per unit length acting on the middle surface of the hydrofoil.

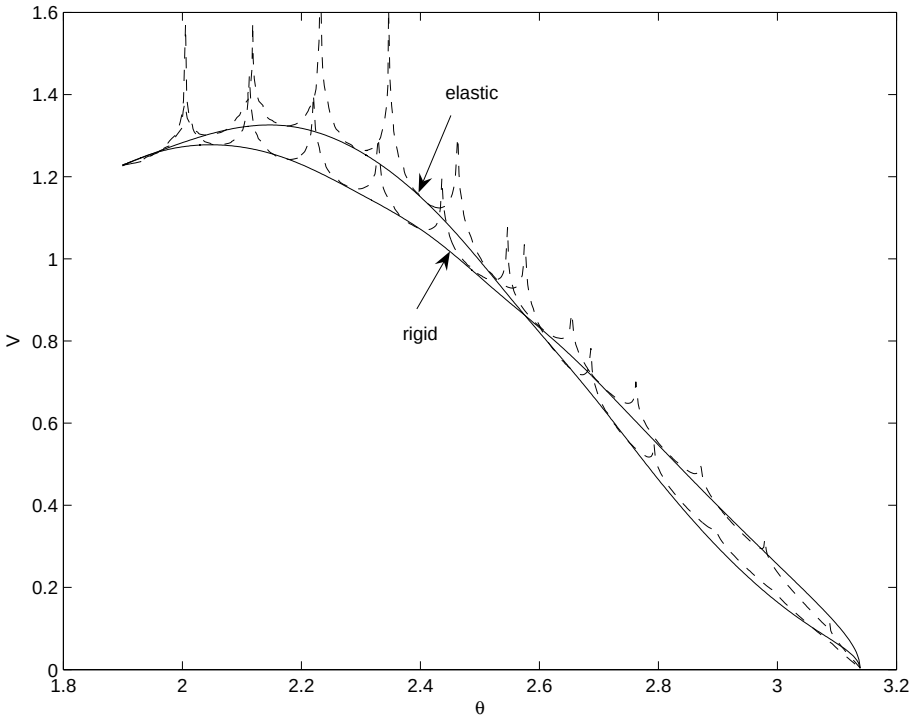

Figure 10: The speed V in the surface of the hydrofoil.

the results of some calculations of the drag coefficient C_X, the cavity length and width versus E. The coefficient C_X, the length and width simultaneously grow when the Young's modulus E grows. The values of E smaller than those used give rise to large deformations and have not been considered.

Conclusions

We have analyzed flow past a supercavitating curvilinear foil. To describe the flow in the rear part of the cavity, the Tulin single-spiral-vortex model was used. The hydrofoil was assumed to be elastic, and the Novozhilov equations of the theory of thin cylindrical shells were employed to model the deformation of the curvilinear foil. To solve the problem, first, we analyzed the single-spiral-vortex model for a rigid polygonal supercavitating hydrofoil. For its solution, we constructed the conformal mapping from the exterior of the unit circle into the flow domain. On applying the Schwarz symmetry principle, the derivative of the mapping function was expressed through the solutions of two Riemann-Hilbert problems. To identify the vertices of the polygon where the jets break away from the foil, we employed the Brillouin-Villat separation condition. The unknown parameters of the conformal mapping were computed on solving approximately by the Newton method a system of transcendental equations. Next, by increasing the number of vertices of a regular N-polygon we approximately solved the cavitation problem for a circular arc and defined pressure q_n on the foil and, therefore, the resulting force per unit length, $q_n - p_c$ (p_c is vapor pressure), acting on the middle surface of the foil. This was needed to state a boundary-value problem for a thin shell subject to normal loading $q_n - p_c$. The elastic problem has been solved exactly for an arc with the clamped-clamped boundary conditions. Then we

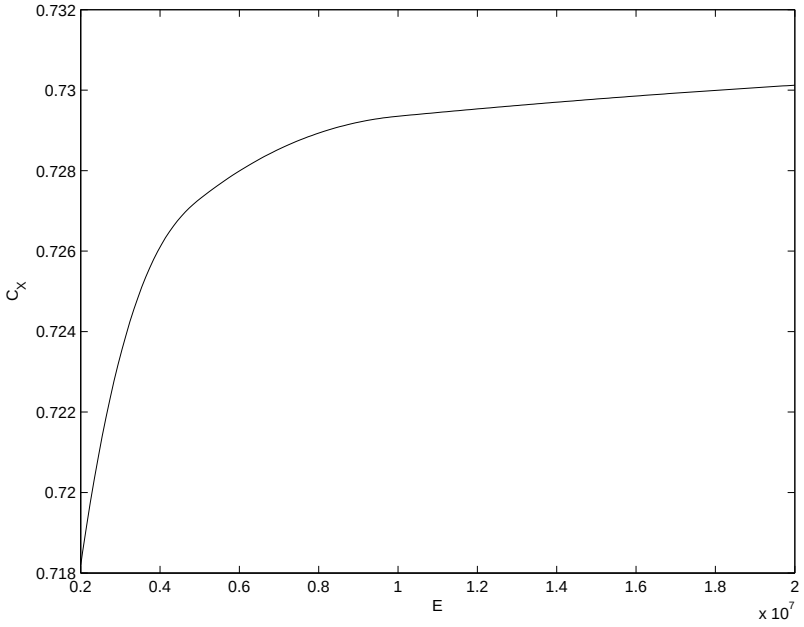

Figure 11: The drag coefficient C_X as a function of the Young's modulus E.

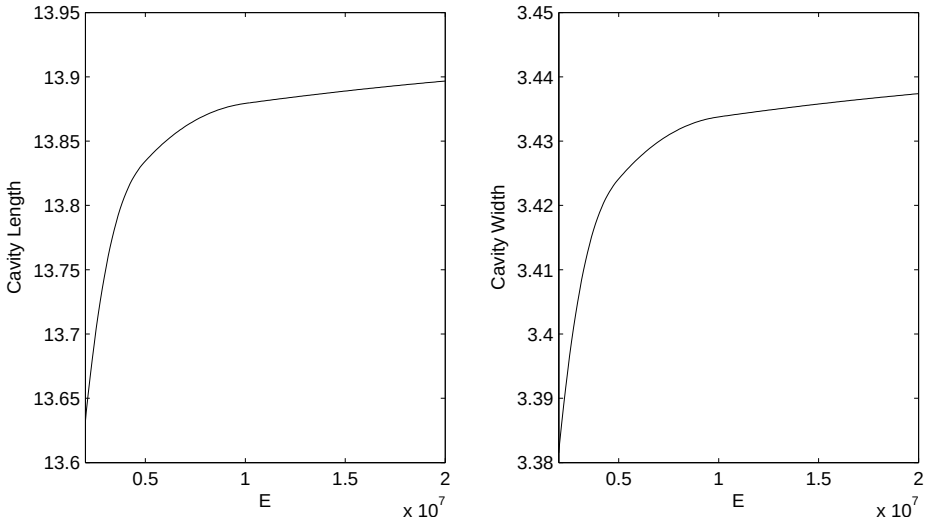

Figure 12: The cavity length and width as functions of the Young's modulus E.

defined the displacements of the foil, reconstructed its new profile and stated a new cavitation problem for the deformed foil. It turns out that the fourth step of the method of successive approximations gives a good accuracy for the displacements and the profile of the deformed foil.

The numerical experiments, among other interesting phenomena, reveal the possible presence of two partial cavities. We have made this prediction on the ground of the existence of two zones, B_rB_1 and B_qB_n (Figure 1), close to the ends of the foil where, first, pressure drops below the vapor pressure p_c and, second, the speed is greater than the constant speed V_c in the cavity boundary. The method presented cannot be directly applied to the nonlinear model problem on a supercavitating circular hydrofoil with two partial cavities. It is feasible, however, to generalize the method by [12] for an elastic hydrofoil and model the partial cavities and the supercavity by using the Efros-Gilbarg-Rock-Kreisel re-entrant jet model and the Kirchhoff-Joukowsky open wake model, respectively.

Acknowledgments. This work was funded by NSF through grant DMS0707724.

References

[1] Y.A. Antipov and V.V. Silvestrov, *Method of Riemann surfaces in the study of supercavitating flow around two hydrofoils in a channel*, Phys. D, 235 (2007), pp. 72-81.

[2] Y.A. Antipov and V.V. Silvestrov, *Double cavity flow past a wedge*, Proc. R. Soc. A, 464 (2008), pp. 3021-3038.

[3] Y.A. Antipov and V.V. Silvestrov, *Circular map for supercavitating flow in a multiply connected domain*, Quart. J. Mech. Appl. Math., 62 (2009), pp. 167-200.

[4] Y.A. Antipov and A.Y. Zemlyanova, *Motion of a yawed supercavitating wedge beneath a free surface*, SIAM J. Appl. Math., 70 (2009), pp. 923-948.

[5] Y.A. Antipov and A.Y. Zemlyanova, *Single- and double-spiral-vortex models for a supercavitating nonsymmetric wedge in a jet*, Proc. Roy. Soc. A, 465 (2009), pp. 3817-3837.

[6] R.E.A. Arndt, *Cavitation*, The Handbook of Fluid Dynamics, Ed. by R.W. Johnson, CRC Press, Boca Raton, 1998.

[7] P. Bassanini and A. Elcrat, *A univalent spiral-vortex model for separated flow past a polygonal obstacle*, ZAMP, 39 (1988), pp. 455-467.

[8] V.F. Bavin, N.Y. Zavadovcki, Y.L. Levkovski and V.G. Mishkevich, *Screw propellers*, Sudostroenie, Leningrad, 1983.

[9] G. Birkhoff and E.H. Zarantonello, *Jets, Wakes, and Cavities*, Academic Press, New York, 1957.

[10] C.E. Brennen, *Cavitation and Bubble Dynamics*, Oxford University Press, Oxford, 1995.

[11] J.P. Breslin and P. Andersen, *Hydrodynamics of ship propellers,* Cambridge University Press, Cambridge, 1994.

[12] A.D. Cox and W.A. Clayden, *Cavitating flow about a wedge at incidence*, J. Fluid Mech., 3 (1958), pp. 615-637.

[13] T.A. Driscoll and L.N. Trefethen, *Schwarz-Christoffel Mapping*, Cambridge University Press, Cambridge, 2002.

[14] P. Eisenberg and M.P. Tulin, *Cavitation*, Handbook of fluid dynamics, Ed. by V. L. Streeter, pp. 12-112-46, McGraw-Hill, New York, 1961.

[15] J.P. Franc and J.M. Michel, *Fundamentals of Cavitation*, Kluwer Academic Publ., New York, 2004.

[16] O. Furuya, *Nonlinear calculation of arbitrary shaped supercavitating hydrofoils near a free surface*, J. Fluid Mech., 68 (1975), pp. 21-40.

[17] D. Gilbarg, *Jets and cavities*, Handbuch der Physic, 9, pp. 311-445, Springer-Verlag, Berlin, 1960.

[18] M.I. Gurevich, *The Theory of Jets in an Ideal Fluid*, Nauka, Moscow, 1979.

[19] J.E. Kerwin, S.A. Kinnas, J.-T. Lee and W.-Z. Shih, *Surface panel method for the hydrodynamic analysis of ducted propellers*, Trans. SNAME, 95 (1987), pp. 93-122.

[20] O.M. Kisilev and E.F. Rapoport, *On streamline flow past an elastic plate*, Mekhanika Zhidkosti i Gaza, no. 4 (1976), pp. 35-42.

[21] O.M. Kisilev and E.F. Rapoport, *On streamline flow past an elastic shell*, Mekhanika Zhidkosti i Gaza, no. 2 (1977), pp. 24-32.

[22] S.A. Kinnas and N.E. Fine, *A numerical nonlinear analysis of the flow around two- and three-dimensional partially cavitating hydrofoils*, J. Fluid Mech., 254 (1993), pp. 151-181.

[23] P.P. Kufarev, *On free-streamline flow about an arc of a circle*, Prikl. Mat. Mech., 16 (1952), pp. 589–598.

[24] B. Larock and R. Street, *Nonlinear solution for a fully cavitating hydrofoil beneath a free surface*, J. Ship Res., 11 (1967) pp. 131-140.

[25] B. Larock and R. Street, *Cambered bodies in cavitating flow - a nonlinear analysis and design procedure*, J. Ship Res., 12 (1968), pp. 1-13.

[26] M.A. Naimark, *Linear differential operators,* F. Ungar Pub. Co, New York, 1967.

[27] V.V. Novozhilov, *Thin shell theory*, Wolters-Noordhoff Publ., Groningen, 1970.

[28] G.N. Pyhteev, *Solution of the inverse problem on plane cavitating flow past curvilinear arc*, Prikl. Mat. Mech., 20 (1956), pp. 589–598.

[29] V.V. Rozhdestvenski, *Cavitation.* Sudostroenie, Leningrad, 1977.

[30] A.G. Terent'ev, *Mathematical Problems of Cavitation*, Chuvash. Gos. Univ., Cheboksary, 1981.

[31] L.N. Trefethen, *Numerical computation of the Schwarz-Christoffel transformation*, SIAM J. Sci. Stat. Comput., 1 (1980), pp. 82-102.

[32] M.P. Tulin, *Supercavitating flows – small perturbation theory*, J. Ship Res., 7, no.3 (1964), pp. 16-37.

[33] T.Y. Wu, *Cavity and wake flows*, Annu. Rev. Fluid Mech., 4 (1972), pp. 243-284.

[34] Y.L. Young and S.A. Kinnas, *Analysis of supercavitating and surface-piercing propeller flows via BEM*, Computational Mech., 32 (2003), pp. 269-280.

[35] Y.L. Young, *Fluid-structure interaction analysis of flexible composite marine propellers*, J. Fluids Structures, 24 (2008), pp. 799-818.